Supplementary Information

SrO-Layer Inserting in Ruddlesden-Popper Sn-based Perovskite Enables Efficient CO_2 Electroreduction towards Formate

Jing Zhao[#,a,b], Peng Zhang[#,a,b], Lulu Li[a,b], Tenghui Yuan[a,b], Hui Gao[a,b], Gong Zhang[a,b], Tuo Wang[a,b], Zhi-Jian Zhao[a,b] and Jinlong Gong[a,b,c,d]*

[a] School of Chemical Engineering and Technology; Key Laboratory for Green Chemical Technology of Ministry of Education, Tianjin University,Tianjin, 300072, China,

[b] Collaborative Innovation Center of Chemical Science and Engineering (Tianjin), Tianjin 300072, China.

[c] Haihe Laboratory of Sustainable Chemical Transformations, Tianjin 300192, China

[d] Joint School of National University of Singapore and Tianjin University, International Campus of Tianjin University, Binhai New City, Fuzhou 350207, China

*Email: jlgong@tju.edu.cn

# These authors contributed equally to this work.

Experimental Procedures

Materials

$SrCO_3$ (99.5%) and SnO_2 (99%) were purchased from Tianjin Guangfu Technology Development Co. Ltd. KOH (95%), $HAuCl_4 \cdot 3H_2O$ (99%) and NaOH (99%) were purchased from Aladdin Industrial Co. Ltd. H_2SO_4 (95-98%) was purchased from Sinopharm Chemical Reagent Co. Ltd. $Na_2S_2O_3$ (99.5%), iso-propyl alcohol (99.8%), and HF (40.0%) were purchased from J&K Scientific Ltd. NH_4F (96.0%), NH_4Cl (99.5%) were purchased from Tianjin Yuanli Technology Development Co. Ltd. (China). Commercially available carbon-based gas diffusion layers (GDLs, AvCarb GDS3250) were purchased from Xima Laya Photo-Electric Technology Co., Ltd., China. All chemical reagents were used as received without further purification. Al_2O_3 polishing powder (0.05 μm), 5 wt% Nafion solution and 99.999% purity carbon dioxide gas were purchased from Gaossunion Technology Co. Ltd., Dupont and Air Liquide, respectively. All aqueous solutions used ultrapure water (18.25 MΩ·cm) as the solvent.

Characterization

The phase structures were characterized X-ray Diffractometer (XRD, Bruker D8 Focus) with Cu Ka radiation (λ = 1.5418 Å) at 40 kV and 40 mA. Transmission electron microscopy (TEM) images were performed on JEOL JEM-2100F, using the Tecnai G2 F20 microscope with an acceleration voltage of 200 kV. Scanning electron microscopy (SEM) images were carried out on Hitachi S-4800 with an acceleration voltage of 5 kV.

Catalyst synthesis

In this work, the $SrSnO_3$ and Sr_2SnO_4 oxides were synthesized via the traditional solid-state reaction route. Stoichiometric amounts of $SrCO_3$ and SnO_2 were weighed and mixed in a ball mill (Nanjing Nanda, QM-3SP4QM) for 2 h using ethanol as the solvent. The obtained mixture was dried at 100 °C for 10 h. The dried mixtures were mixed using agate mortar then calcined at 900 °C and 1200 °C in ambient air for 12 h to obtain a single phase of $SrSnO_3$ and Sr_2SnO_4, respectively. The control sample of SnO_2 underwent the same procedure and was calcined at 900 °C for 5 h.

Operando Raman spectroscopy experiments

Operando Raman Spectroscopy was carried out using a Raman spectrometer (LabRAM HR Evolution, Horiba Jobin Yvon). The Raman spectroscopy was recorded in a custom-designed flow cell (Figure S14), which was supplied by Gaossunion Co., Ltd., Tianjin. A three-electrode configuration (PEEK wrapped electrodes, Ag/AgCl electrode and Pt wire were served as the working electrode, reference electrode and counter electrode) was utilized in the flow cell for electrochemical experiments. The anion exchange membrane (AEM, FAA-3-PK-75, Fumatech) was used to separate the working electrode from the counter

electrode, to avoid mixing of products. The excitation wavelength was a visible light laser (λ = 532 nm). The CO_2RR was performed at −0.58 to −1.28 V *vs.* RHE in 0.5 M $KHCO_3$ solution on different catalysts, and the Raman signal was recorded after the reaction for each potential, when the current density retained a steady state, using workstation (Compact-Stat. e20250, IVIUM) to supply potential.

Operando ATR-SEIRAS experiments

Operando ATR-SEIRAS was recorded by using the FT-IR spectrometer (is50, Nicolet). The *operando* electrochemical cell was based on the design of Xu et al.[1] and manufactured by Gaossunion Co., Ltd., Tianjin. An Si prism, Ag/AgCl electrode and Pt foil were served as the working electrode, reference electrode and counter electrode. The Si prism covered with gold film by chemical deposition and more detailed about the preparation process could be found in Deng.[2] Subsequently, the catalyst suspension (3 mg/mL) was dropped onto the surface. Later, 20 ml electrolyte was bubbled with CO_2 for 30 min before the test. The background was taken at 0.1 V *vs.* RHE Ar-saturated electrolyte before each test. We acquired the spectra by LSV, the final spectra were acquired with resolution of 4 cm^{-1} by accumulating 2 scans during the potential interval from −0.38 to −1.38 V *vs*. RHE.

CO_2RR performance test in H-cell

The electrochemical test was carried out in a three-electrode system, Ag/AgCl and Pt foil were served as reference and counter electrodes, respectively. Electrode potential was provided with an Ivium electrochemical workstation. The performance CO_2RR was detected in a homemade H-cell (30 ml of single cell) with an ion-exchange membrane (Nafion). The 0.5 M $KHCO_3$ electrolyte was bubbled with CO_2 for 30 min before the electrochemical reaction. The CO_2 flow rate was controlled by a mass flow meter (MC-Series, Alicat Scientific) with a flow rate control of 20 sccm. After the amount of e^- flowing through the cathode has accumulated to 30 C, the products were quantified. All potentials were not *iR* corrected.

CO_2RR performance test in flow cell

1 M KOH solution was served as both the catholyte and the anolyte in a homemade flow cell configuration (Gaossunion Co., Ltd.) equipped with a gas diffusion layer, reference electrode (Hg/HgO) and nickel foam anode. The CO_2 flow rate is controlled by a mass flow meter, and the inlet flow rate is controlled at 40 sccm. To ensure the accuracy of the product selectivity calculation, another flow meter was used to accurately measure the outlet CO_2 flow rate, because OH^- can react with CO_2 to form HCO_3^- or CO_3^{2-}. The current fluctuations are due to the addition of electrolyte to avoid the formation of (bi)carbonate salts on the diffusion layer. After the amount of e^- flowing through the cathode has accumulated to 50 C, the products were quantified. All potentials were not *iR* corrected.

Analysis of CO_2RR products

The gaseous products were delivered to the gas chromatography (GC, Ruimin GC, 2060) for on-line analysis. CO and H_2 were detected by a flame ionization detector (FID) and thermal conductivity detector (TCD), respectively. The liquid products were quantified by ^{1}H NMR and ^{1}H spectra were performed on Bruker (Advance). 1 mL of electrolyte (after reaction) was mixed with 0.1 mL mixture of 10 mL D_2O and 0.01 mL dimethyl sulfoxide (DMSO) and were analyzed using a 400 MHz NMR spectrometer.

Computational details

Density functional theory (DFT) calculations were employed through the Vienna ab initio Simulation Package (VASP) code in conjunction with the computational hydrogen electrode (CHE) model.[3,4] The surface energy of different $SrSnO_3$ surfaces were calculated according to the following equation.

$$\gamma = E_{(cut)} + E_{(relax)} = \frac{1}{2A}\left[E_{slab}^{unrelax} - nE_{bulk}\right] + \frac{1}{A}\left[E_{slab}^{relax} - E_{slab}^{unrelax}\right]$$

$$E_{slab}^{unrelax}: Energy\ of\ single\ point$$

In all calculations, the model surfaces were conducted using a four-layer (2×2) periodic slab, where the two bottom layers were kept fixed, and the Monkhorst-Pack k-mesh of 3×3×1 for Sr_2SnO_4(002) with SrO as well as SnO layer, and $SrSnO_3$(001), 4×3×1 for SnO_2(110) were adopted for integrations over the Brillouin zone for all systems.[5] Besides, at least 15 Å vacuum space was set between the slabs to the periodic images in the vertical direction. The generalized gradient approximation (GGA) was adopted in the form of the PBE functional and projector augmented wave (PAW) pseudopotentials to describe the electron exchange and correlation effects.[6] Cut-off energy of 400 eV and atomic force convergence of 0.02 eV/Å were employed. In addition, the spin polarization scheme was adopted for all calculations. The free energy for each intermediate state was calculated through $G = E_{DFT} + ZPE + \delta_{H0} - TS$, where E_{DFT} is the DFT total energy, ZPE is the zero-point vibrational energy, δ_{H0} is the integrated heat capacity, T is the reaction temperature and S is the entropy. For gas and liquid phase species, the δ_{H0} and entropy S at 298.15 K were obtained from the references or adsorbates, the entropy was calculated with the Harmonic oscillator approximation.[8,9] In this study, we calculated both CO_2RR and HER. The asterisk (*) denotes the substrate. The whole process including the CO_2RR to HCOOH or CO, and the competing HER to H_2 consists of the following main steps:

(1) $CO_2\,(g) + * + H^+\,(aq) + e^- \rightarrow {}^*OCHO$, $\Delta G_{R1} = G_{*OCHO} - 1/2G_{H2} - G_{CO2}$

(2) ${}^*OCHO + H^+\,(aq) + e^- \rightarrow HCOOH\,(aq)$, $\Delta G_{R2} = G_{HCOOH}\,(aq) - 1/2G_{H2} - G_{*OCHO}$

(3) $CO_2\,(g) + * + H^+\,(aq) + e^- \rightarrow {}^*COOH$, $\Delta G_{R3} = G_{*COOH} - 1/2G_{H2} - G_{CO2}$

(4) ${}^*COOH + H^+\,(aq) + e^- \rightarrow CO\,(g) + H_2O\,(l)$, $\Delta G_{R4} = G_{CO} + G_{H2O} - 1/2G_{H2} - G_{*COOH}$

(5) $H^+\,(aq) + e^- + * \rightarrow {}^*H$, $\Delta G_{R5} = G_{*H} - 1/2G_{H2}$

The crystal orbital Hamilton population (COHP) analysis was conducted through the Lobster 3.2.0 code and the Integrating the COHP (iCOHP) up to the Fermi level was calculated to compute the pair-wise interatomic interaction strength.[7]

Supplementary Figures

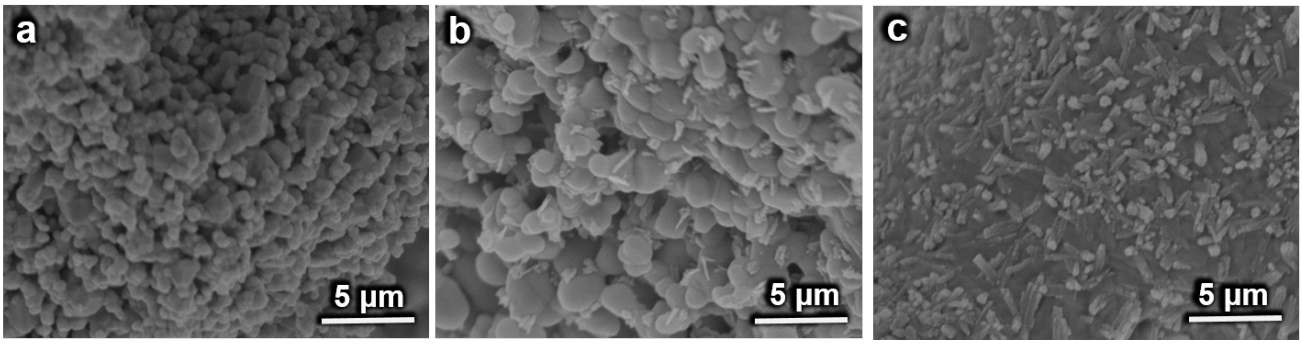

Figure S1. SEM images of (a) SnO_2, (b) $SrSnO_3$ and (c) Sr_2SnO_4.

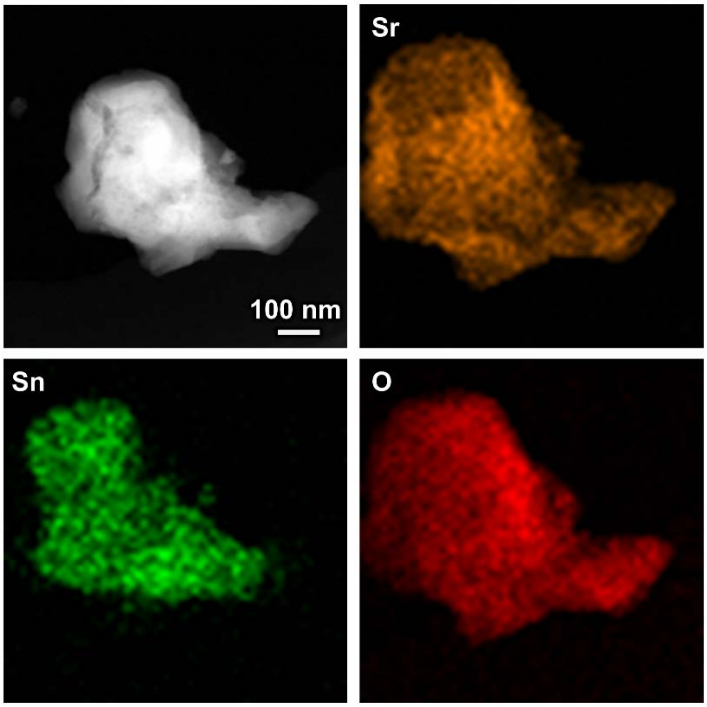

Figure S2. EDS mapping images of $SrSnO_3$.

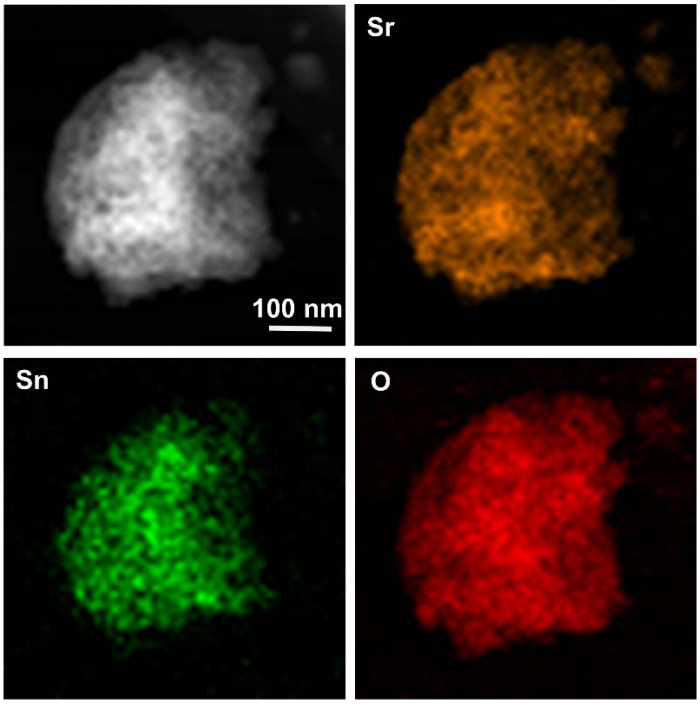

Figure S3. EDS mapping images of Sr_2SnO_4.

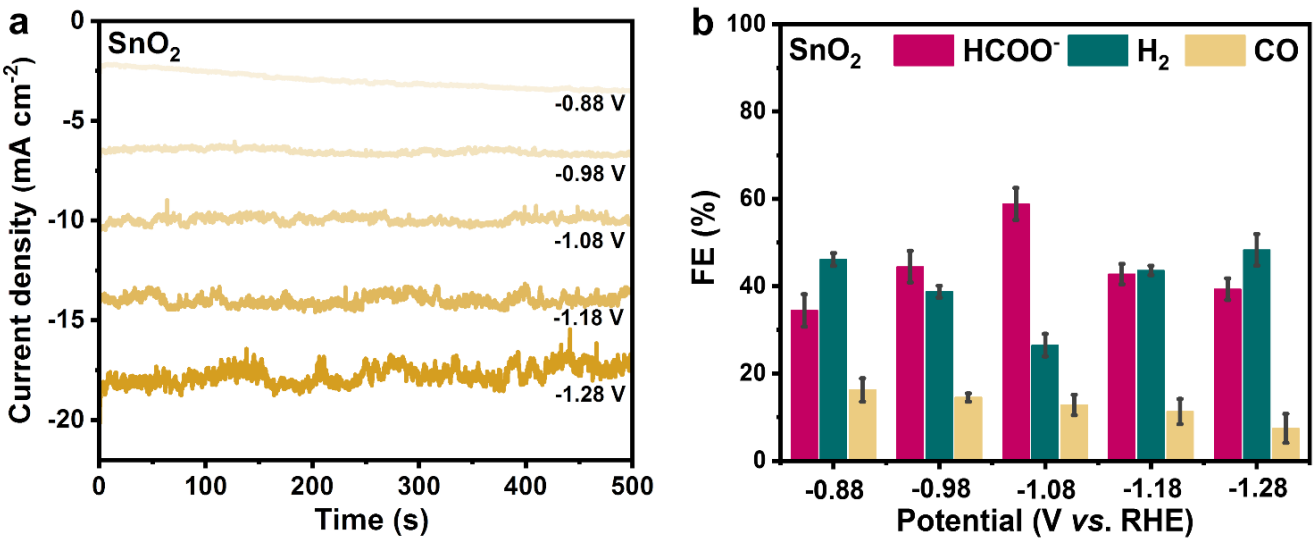

Figure S4. (a) Chronoamperometric curves and (b) FEs for products of SnO_2 at different potentials.

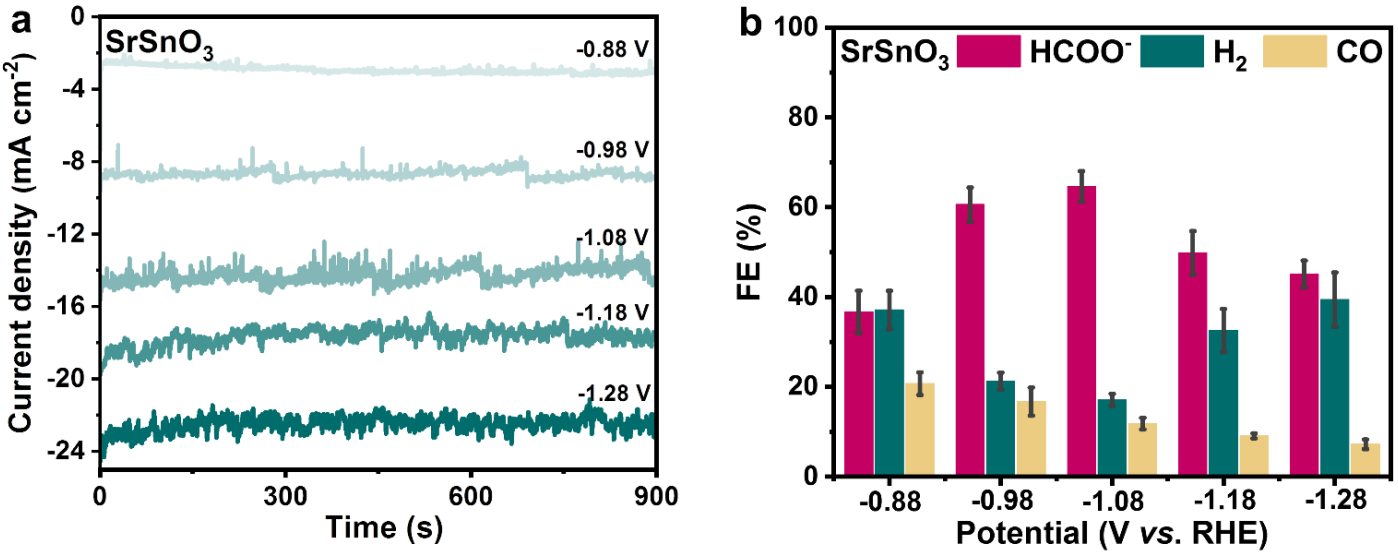

Figure S5. (a) Chronoamperometric curves and (b) FEs for products of $SrSnO_3$ at different potentials.

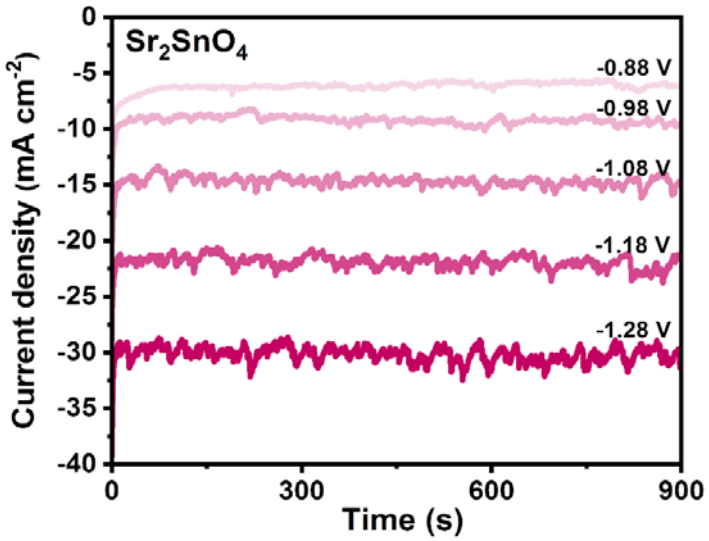

Figure S6. Chronoamperometric curves of Sr_2SnO_4 at different potentials.

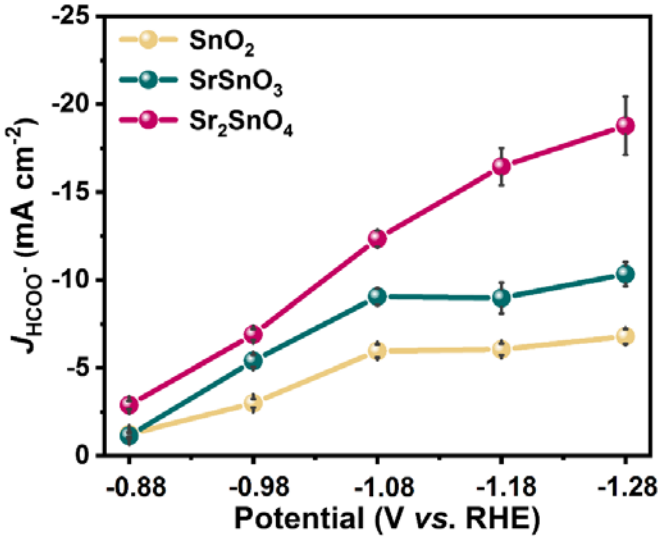

Figure S7. Partial current density of $HCOO^-$ for SnO_2, $SrSnO_3$ and Sr_2SnO_4.

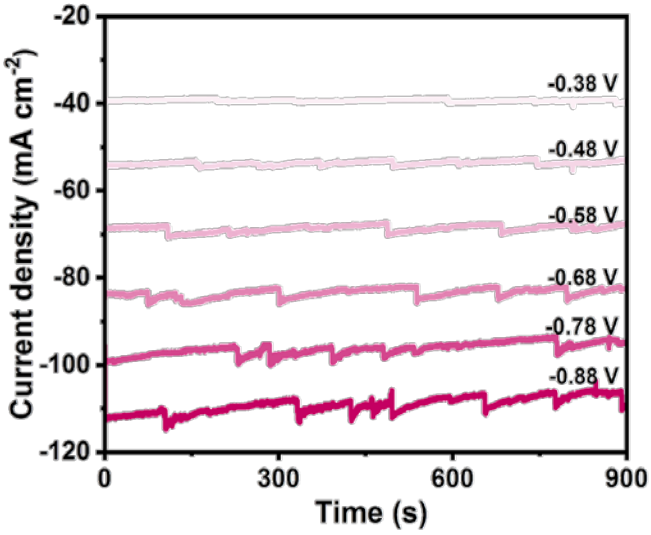

Figure S8. Chronoamperometric curves for Sr_2SnO_4 in a flow cell at different potentials.

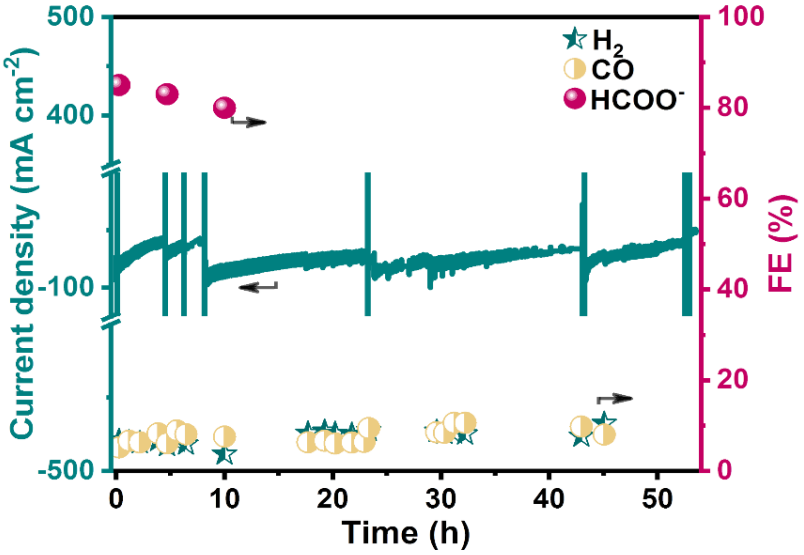

Figure S9. Long-term stability test of Sr_2SnO_4 for CO_2RR at the potential of −0.68 V *vs.* RHE in a flow cell.

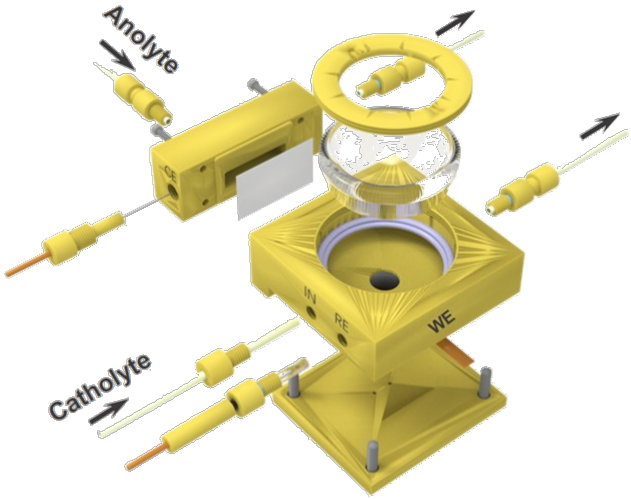

Figure S10. Electrochemical cell for collecting *operando* Raman spectra.

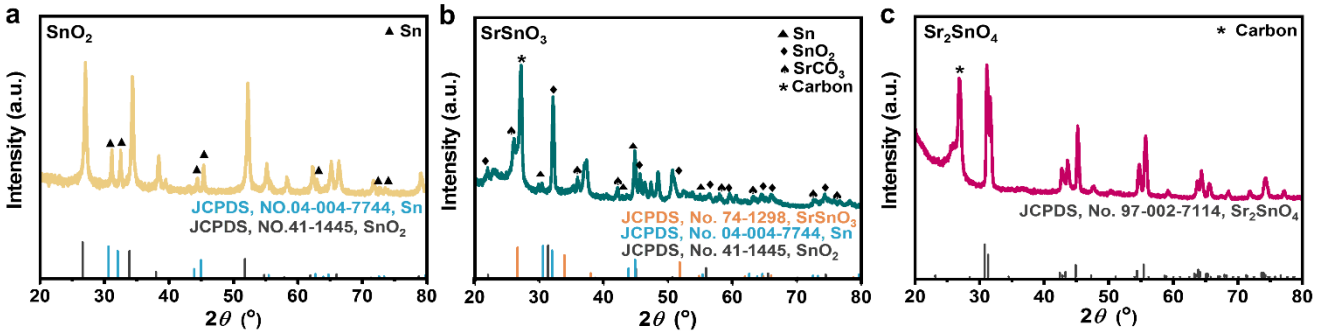

Figure S11. XRD patterns of (a) SnO_2, (b) $SrSnO_3$ and (c) Sr_2SnO_4 after stability tests.

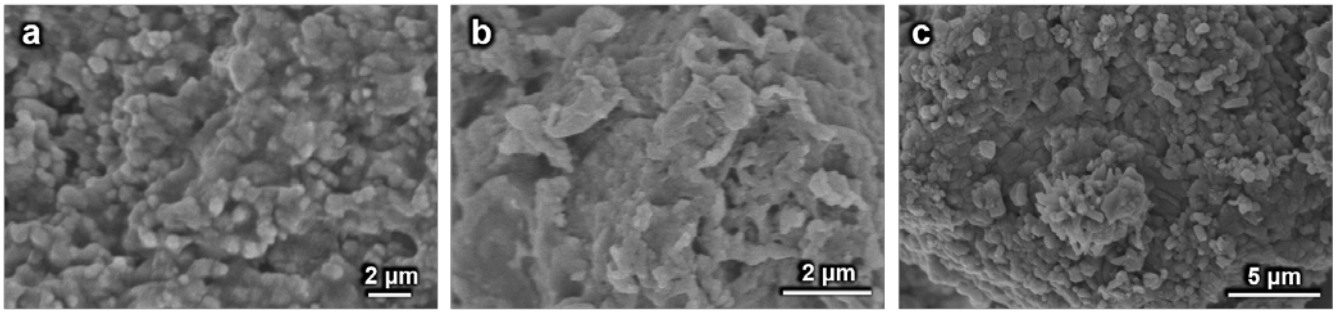

Figure S12. SEM images of (a) SnO_2, (b) $SrSnO_3$ and (c) Sr_2SnO_4 after CO_2RR stability test.

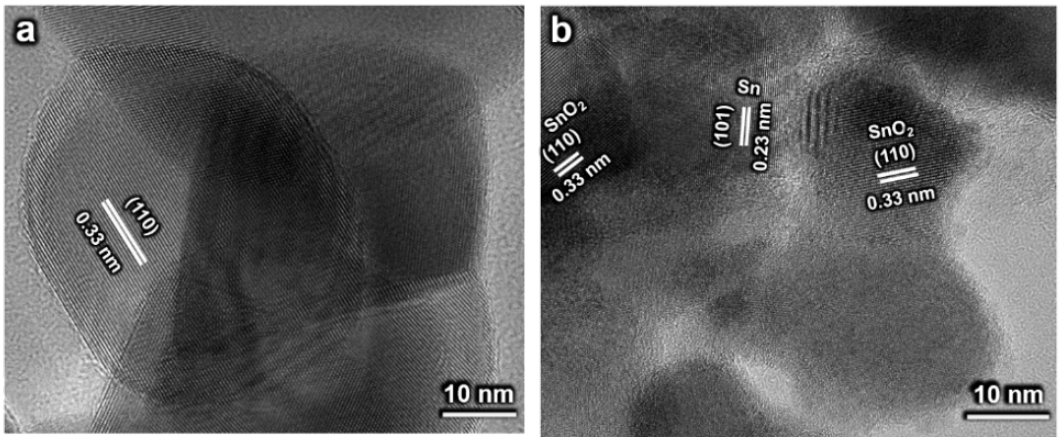

Figure S13. HRTEM images of SnO_2 (a) before and (b) after CO_2RR stability test.

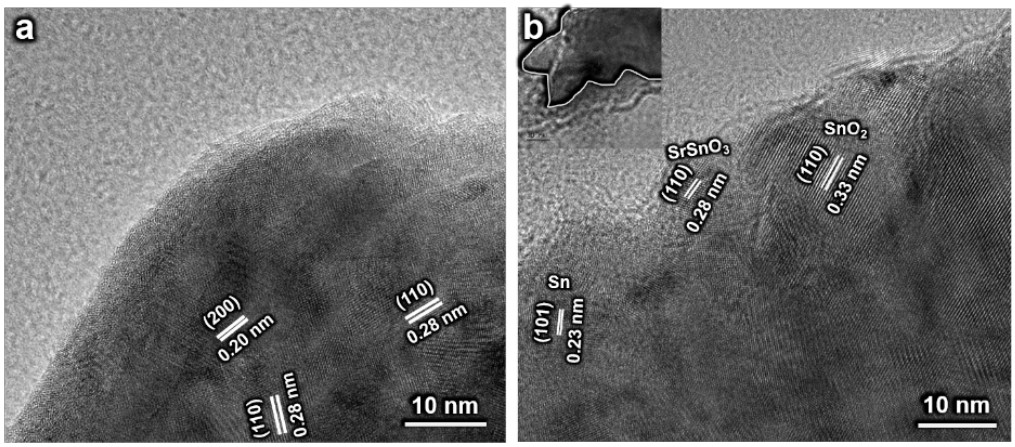

Figure S14. HRTEM images of $SrSnO_3$ (a) before and (b) after CO_2RR stability test.

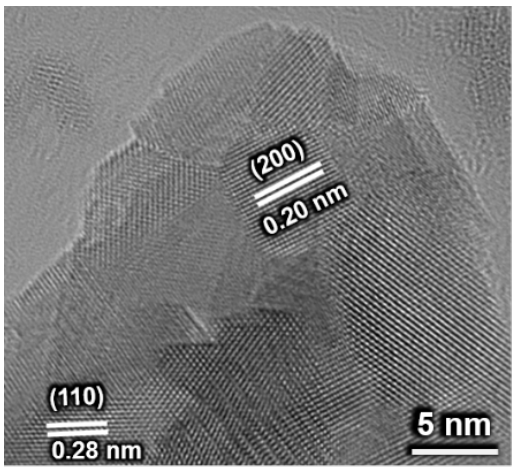

Figure S15. HRTEM image of Sr_2SnO_4 after CO_2RR stability test.

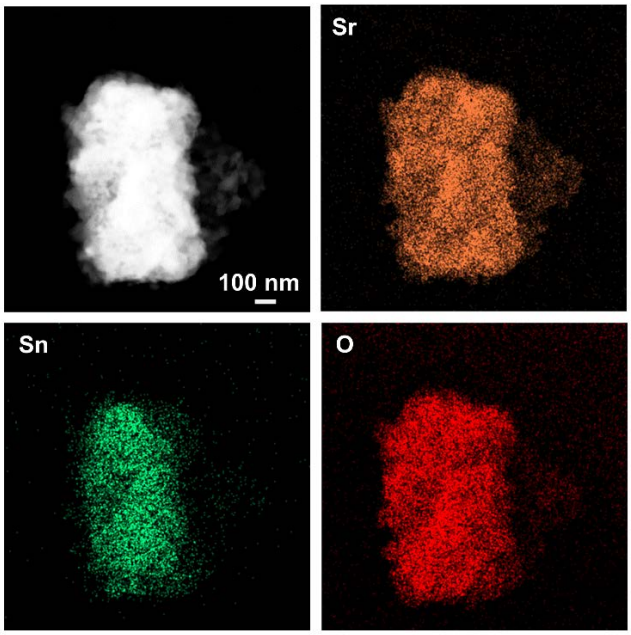

Figure S16. EDS mapping images of Sr_2SnO_4 after CO_2RR stability test.

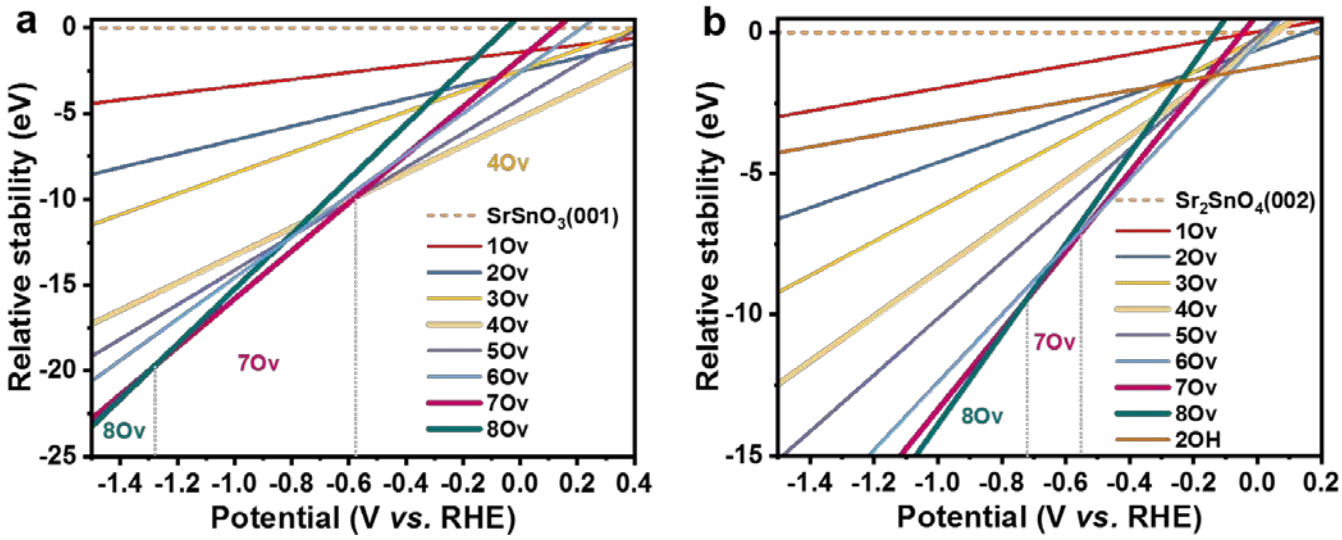

Figure S17. Surface phase diagrams of (a) $SrSnO_3$ and (b) Sr_2SnO_4.

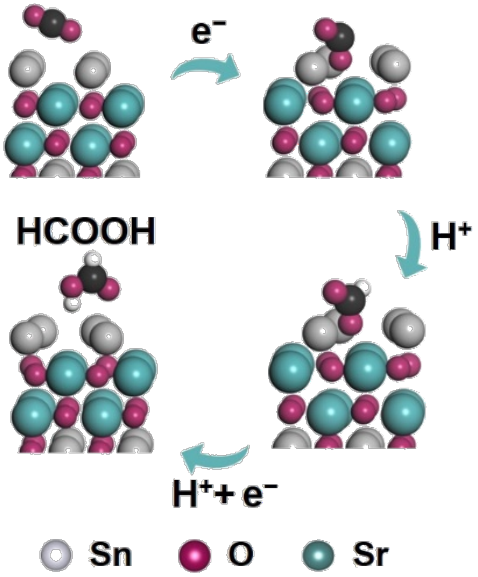

Figure S18. Illustration of the reaction pathway for CO_2RR to HCOOH over Sr_2SnO_4(002).

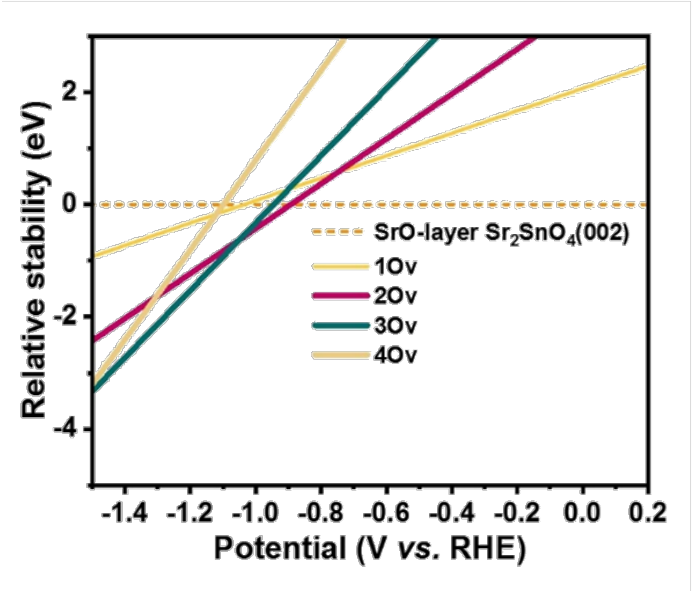

Figure S19. Surface phase diagrams of the SrO-layer in $Sr_2SnO_4(002)$. The SrO-layer in $Sr_2SnO_4(002)$ is thermodynamically stable.

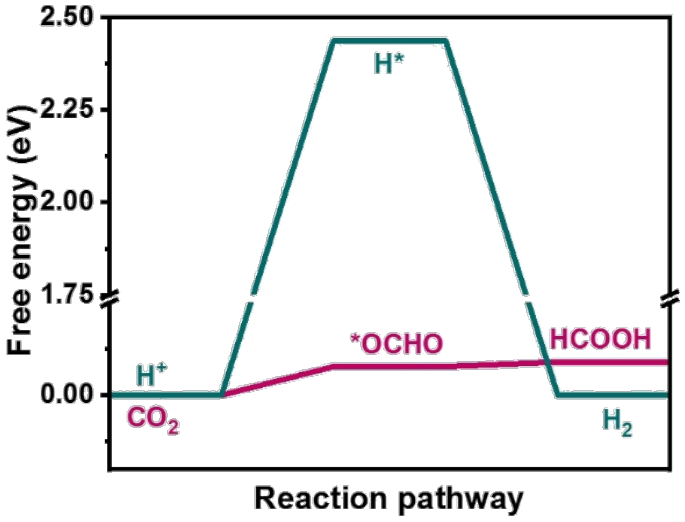

Figure S20. The calculated free energy for HCOOH and H_2 for the SrO-layer in Sr_2SnO_4(002).

Table S1. The CO_2RR performance of the state-of-the-art electrocatalysts towards formate.

Catalyst	Electrolyte	Potential	FE (%)	$J_{formate}$ (mA/cm^2)	Cell type	References
Nano SnO_2/carbon	0.1 M $NaHCO_3$	−1.80 V *vs*. SCE	93.6	9.5	H-cell	*J. Am. Chem. Soc*. 2014,136,1734
Cu_2SnS_3 nanosheets	0.5 M $KHCO_3$	−0.80 V *vs*. RHE	83.4	~20.0	flow cell	*Angew. Chem. Int. Ed.* 2021,60,1
Chainlike Mesoporous SnO_2	0.1 M $KHCO_3$	−1.06 V *vs*. RHE	82.0	~13	H-cell	*ACS Appl. Energy Mater.* 2019,2,3081
Sn quantum sheets in graphene	0.1 M $NaHCO_3$	−1.80 V *vs*. SCE	89.0	18.8	H-cell	*Nat. Commun*. 2016,7,12697
SnO_2/carbon cloth	0.5 M $NaHCO_3$	−1.60 V *vs*. Ag/AgCl	87.0	~45.0	H-cell	*Angew. Chem. Int. Ed.* 2016,55,1
Reduced SnO_2 porous nanowires	0.1 M $KHCO_3$	−0.80 V *vs*. RHE	80.0	4.8	H-cell	*Angew. Chem. Int. Ed.* 2017,56,3645
Mesoporous SnO_2 nanosheets	0.5 M $KHCO_3$	−0.90 V *vs*. RHE	83.0	~16.0	H-cell	*J. Mater. Chem. A* 2019,7,1267
$SrSnO_3$ bulk	0.5 M $NaHCO_3$	−1.00 V *vs*. RHE	73.8	~8.0	H-cell	*Nano Energy* 2019,62,861
SnO_2 nanosheets	0.1 M $KHCO_3$	−1.60 V *vs*. RHE	73.0	~7.3	H-cell	*Adv. Energy Mater.* 2018,8,1801230
Flame spray pyrolysis-SnO_2	0.1 M $KHCO_3$	−1.10 V *vs*. RHE	85.0	20.1	H-cell	*Adv. Sci.* 2019,6,1900678
Bi-doped SnO	0.1 M $KHCO_3$	−1.10 V *vs*. RHE	93.0	11.2	H-cell	*Electrochim. Acta* 2020,332,135457
Bi Dendrite	0.5 M $KHCO_3$	−0.74 V *vs*. SCE	89.0	2.3	H-cell	*ACS Catal.* 2017,7,5071

Bi–Sn foam	0.1 M $KHCO_3$	−1.20 V *vs*. RHE	82.0	20.5	H-cell	*Nano Lett.* 2020,20,4403
$Bi_2O_2CO_3$ nanosheets	0.5 M $NaHCO_3$	−0.70 V *vs*. RHE	85.0	9.4	H-cell	*Angew. Chem. Int. Ed.* 2018,57,13283
Bi nanosheets	0.5 M $NaHCO_3$	−1.74 V *vs*. SCE	~100.0	24.0	H-cell	*Nat. Commun.* 2018,9,1320
Oxide-derived Pb	0.5 M $NaHCO_3$	−0.75 V *vs*. RHE	~100.0	NA	H-cell	*ACS Catal.* 2015,5,465
High-vacancy InO_x	0.5 M $NaHCO_3$	−0.70 V *vs*. RHE	91.7	~4.6	H-cell	*Angew. Chem. Int. Ed.* 2019,58,5609
S-In_2O_3 derived In	0.5 M $KHCO_3$	−0.98 V *vs*. RHE	93.0	53.0	H-cell	*Nat. Commun.* 2019,10,892
$Pd_{70}Pt_{30}$/C nanoparticles	0.1 M KH_2PO_4/0.1 M K_2HPO_4	−0.40 V *vs*. RHE	90.0	4.5	H-cell	*ACS Catal*. 2015,5,3916
Pd-Sn alloy	0.5 M $KHCO_3$	−0.26 V *vs*. RHE	~100.0	NA	H-cell	*Angew. Chem*. 2017,129,12387
Sr_2SnO_4	1.0 M KOH	−0.68 V *vs*. RHE	84.5	~70.0	flow cell	*This work*
Sr_2SnO_4	0.5 M $KHCO_3$	−1.08 V *vs*. RHE	83.7	12.4	H-cell	*This work*

Table S2. The surface energy of diffrerent $SrSnO_3$ surfaces.

Surface	001	110	200	220	310
Surface energy (meV/Å^2)	60.53	96.75	63.81	130.27	64.72

Table S3. Calculated oxygen vacancy formation energy of SnO_2.

$\Delta E(O_{v,\,bri})$	$\Delta E(O_{v1,\,bulk})$	$\Delta E(O_{v2,\,bulk})$	$\Delta E(O_{v,\,ip})$
0.43 eV	1.90 eV	1.83 eV	1.15 eV

Bridging oxygen vacancy ($O_{v,\,bri}$)

Bulk oxygen vacancy ($O_{v,\,bulk}$)

In-plane oxygen vacancy ($O_{v,\,ip}$)

Table S4. Calculated oxygen vacancy formation energy of $SrSnO_3$ and Sr_2SnO_4.

Sample	**$\Delta E(1O_{v,\,sur})$**	**$\Delta E(O_{v,\,bulk})$**
$SrSnO_3$	−1.41 eV	0.94 eV
Sr_2SnO_4	−0.03 eV	1.72 eV

Surface oxygen vacancy ($O_{v,\,sur}$)

References

1. J. Li, X. Chang, H. Zhang, A. S. Malkani, M. J. Cheng, B. Xu and Q. Lu, *Nat. Commun.*, 2021, **12**, 3264.
2. W. Deng, L. Zhang, L. Li, S. Chen, C. Hu, Z.-J. Zhao, T. Wang and J. Gong, *J. Am. Chem. Soc.*, 2019, **141**, 2911-2915.
3. G. Kresse and J. Furthmüller, *Phys. Rev. B* 1996, **54**, 11169-11186.
4. A. A. Peterson, F. Abild-Pedersen, F. Studt, J. Rossmeisl and J. K. Nørskov, *Energy Environ. Sci.*, 2010, **3**, 1311-1315.
5. H. J. Monkhorst and J. D. Pack, *Phys. Rev. B*, 1976, **13**, 5188-5192.
6. G. Kresse and D. Joubert, *Phys. Rev. B*, 1999, **59**, 1758-1775.
7. J. A. Dean, in Lang's Handbook of Chemistry 13th Ed. McGraw-Hill Professional, Columbus, America, 1998, Sec. 6.
8. R. Dronskowski and P. E. Blöchl, *J. Phys. Chem.*, 1993, **97**, 8617-8624.
9. V. L. Deringer, A. L. Tchougreeff and R. Dronskowski, *J. Phys. Chem. A*, 2011, **115**, 5461-5466.